Performance assessment of a 5GNR D-band CMOS transceiver with phase noise impairments

Yaya Bello, David Demmer, Jean-Baptiste Dore, Nicolas Cassiau, José Luis Gonzalez Jimenez, Abdelaziz Hamani, Cedric Dehos, Alexandre Siligaris

Performance Assessment of a 5GNR D-Band CMOS Transceiver with Phase Noise Impairments

Yaya Bello, David Demmer, Abdelaziz Hamani, Alexandre Siligaris, Cedric Dehos,
Nicolas Cassiau, Jean-Baptiste Doré, José Luis González-Jiménez
CEA-Leti, Univ. Grenoble Alpes, F-38000 Grenoble, France
{yaya.bello, jean-baptiste.dore}@cea.fr

***Abstract*—Sub-THz bands offer a strong potential with their wide available bandwidths, which makes them a promising enabler for 6G. However, the channel propagation is challenging in those bands because of severe path loss attenuation. Hardware impairments are also strong especially phase noise (PN). Besides, silicon based components, which prevail in mobile systems thanks to their low production costs, reach their limits in such high frequencies. There is thus a need for specific solutions for both system designs and signal processing techniques. The contributions of the proposed work are multiple: (i) based on a CMOS D-Band transceiver, we measure and derive the stochastic properties of the transceiver PN and, (ii) we investigate and evaluate the performance of signal processing PN estimation and compensation techniques, with the measured PN for OFDM and DFT-s-OFDM waveforms. We demonstrate that the use of the proposed algorithm based on the statistic properties of the correlated nature of the PN, leads to a significant performance gain in DFT-s-OFDM systems. We consider a real measurement of the PN power spectral density and standard and extended 5G-NR numerologies.**

***Index Terms*—sub-THz, OFDM, DFT-s-OFDM, Phase Noise**

I. Introduction

The deployment of 5G network has enabled to connect a tremendous number of devices and to collect a massive quantity of data. Consequently, recent technological advances have brought to life new applications yet inconceivable a decade ago such as machine learning or digital twins. Our society is turning into data-driven and this digital transformation is pushing the mobile networks to their limits. 6G will emerge to satisfy the requirements not met by 5G [1].

Its potential will be realized by accessing upper mmWave and sub-THz bands which offer large available bandwidths [2]. However, ensuring a reliable wireless communication above 100 GHz is challenging for both radio system designers and developers of signal processing modules. Indeed, regarding transceiver design, complementary metal-oxide-semiconductor (CMOS) technology has prevailed in conventional mobile systems as it provides strong integration and good energy-efficiency with low production costs. Yet, CMOS-based designs above 100 GHz is not straightforward because it is difficult to simultaneously achieve: (i) high power, (ii) wideband and (iii) low noise figure. Over the past decades, continuous scaling of CMOS technology has paved the way to fully integrated wireless systems operating above 100 GHz [3]–[5].

In addition, as in 5G new radio (5G-NR), the 3rd generation partnership project (3GPP) thinks about the implementation of 5G-NR multicarrier waveforms such as orthogonal multiplexing division multipexing (OFDM) and discrete Fourier transform-spread-OFDM (DFT-s-OFDM) in wireless communications for the next 6G. Nevertheless, the phase noise (PN) level in sub-THz bands causes some drawbacks which limit the achievable performance [6]. In terms of waveform and signal processing, two solutions are proposed to enhance radio frequency (RF) system performance against the effects of PN. The first is to propose robust waveforms to PN, compatible with the multicarrier framework of 3GPP. The authors of [7] [8] show how the concept of numerology can be extended to increase the intercarrier spacing (ICS) and make the OFDM waveform more robust to PN. The second method consists in proposing digital signal processing techniques and some recent works in the literature propose intercarrier interference (ICI) cancellation techniques for OFDM [9]–[12] and post-fast Fourier transform (FFT) PN estimation algorithms for DFT-s-OFDM [13], [14].

The contributions of the paper are: (i) Provide a comprehensive analysis of channel bonding RF architecture for D-Band transceiver, (ii) Give the PN characteristics of a D-Band CMOS transceiver and compare them with the generic 3GPP model widely used in the literature, (iii) Assess the performance of a 5G-NR OFDM based waveform under realistic PN model.

Notations: Underlined lower boldface letters, $\underline{\mathbf{a}}$, indicate column vectors, with $\underline{\mathbf{a}}^{(k)}$ the k^{th} element of the column vector. Higher boldface letters $\mathbf{A}$ denote matrices where $\mathbf{A}^{(i,k)}$ is the element at the i^{th} row and k^{th} column of $\mathbf{A}$. The term $E[\cdot]$ denotes the expectation operator. The Moore-Penrose pseudo-inverse $\mathbf{A}^{\dagger}$ is defined as $\mathbf{A}^{\dagger} = \left(\mathbf{A}^H\mathbf{A}\right)^{-1}\mathbf{A}^H$ where the symbol $(\cdot)^H$ denotes the Hermitian operator. The operator $\odot$ represents the Hadamard product. $\underline{\mathbf{N}}_X$ indicates column vectors of size X, containing the scalar $\mathbf{N}$ in all rows. $\mathbf{N}_X$ indicates matrices of size $X \times X$ that fully contain the number $\mathbf{N}$. $\mathbf{F}_X$ is the discrete Fourier transform (DFT) matrix of size X defined as $\mathbf{F}_X^{(i,k)} = \frac{1}{\sqrt{X}} e^{-j2\pi\frac{(i-1)(k-1)}{X}}$.

II. System Model

A. Physical (PHY) Layer

OFDM is a widely used waveform standardized in 4G and 5G-NR for wireless system [15]. 5G-NR introduced the concept of numerology [15] which consists in increasing the ICS to cope with the mobility and to take advantage of millimeter wave spectrums. The ICS is defined as $\Delta_f =$

This work has been partially funded by Horizon Europe project CORENEXT.

TABLE I
NUMEROLOGY SCALING FRAMEWORK ACCORDING TO 5G-NR, INSPIRED FROM [7].

	μ	ICS [kHz]	NFFT	Sampling Frequency [MHz]	80% of Bandwidth [MHz]
5G-NR	0	15	4096	61.44	49.15
	1	30	4096	122.88	98.30
	2	60	4096	245.76	196.61
	3	120	4096	491.52	393.22
	4	240	4096	983.04	786.43
	5	480	4096	1966.08	1572.86
	6	960	4096	3932.16	3145.73
Option 1	7	1920	4096	7864.32	6291.46
	8	3840	4096	15728.64	12582.91
	9	7680	4096	31457.28	25165.82
	10	15360	4096	62914.56	50331.65
Option 2	7	1920	2048	3932.16	3145.73
	8	3840	1024	3932.16	3145.73
	9	7680	512	3932.16	3145.73
	10	15360	256	3932.16	3145.73

$15 \times 2^{\mu}$ kHz, where μ is the numerology. This technique maintains compatibility with the 3GPP framework in terms of channel coding, synchronization, channel estimation, physical channel assignment, etc. Despite the line-of-sight (LoS) propagation and the low frequency selectivity of the channel in the sub-THz bands (by considering high gain and highly directive antennas [16]), OFDM-based waveforms could be particularly interesting for dealing with frequency-dependent RF degradation (in-band attenuation), carrier-based digital beamforming in combination with a phased array and OFDM access (OFDMA). Nevertheless, the peak-to-average power ratio (PAPR) of OFDM is high, which puts a lot of constraints on the power amplifier (PA) [17].

As the efficiency of high frequency PAs is low, it seems essential to have a low PAPR waveform. If the advantages of OFDM have to be maintained, the use of DFT-s-OFDM seems to be a good compromise. As OFDM, the DFT-s-OFDM is standardized in 4G and 5G-NR in uplink transmissions. By performing a full band Fourier transform, the signal envelope of a DFT-s-OFDM waveform tends towards the behavior of a single-carrier waveform and thus, leads to a low PAPR compared to OFDM, while allowing OFDM compatible processing [18]. However, the penalty is an increase of complexity.

To address the very wide frequency bands offered by sub-THz, several approaches can be considered. Firstly, by stretching the bandwidth, *i.e.* increasing the addressable spectrum by increasing the numerology [8]. As shown in TABLE I, a numerology of 10 allows 50 GHz of spectrum to be addressed, while considering the 4096 FFT size defined in 5G-NR. However, this configuration seems difficult to realize in practice as it requires fast conversion systems that are far beyond the current limits [19]. A second option is to address the entire bandwidth by carrier aggregation. In this case, the constraints on conversion are limited at the cost of duplicating the components. To make the waveforms robust to PN, it is necessary to have large ICS, and therefore a high numerology. When the PN-induced distortions become critical and limit the system performance, "Option 2" of TABLE I could be interesting. This option consists in increasing the numerology by controlling the sampling frequency at the cost of reducing the number of addressable resource block (RB). It is the approach we propose to implement larger numerologies, *i.e.* $\mu \geq 6$.

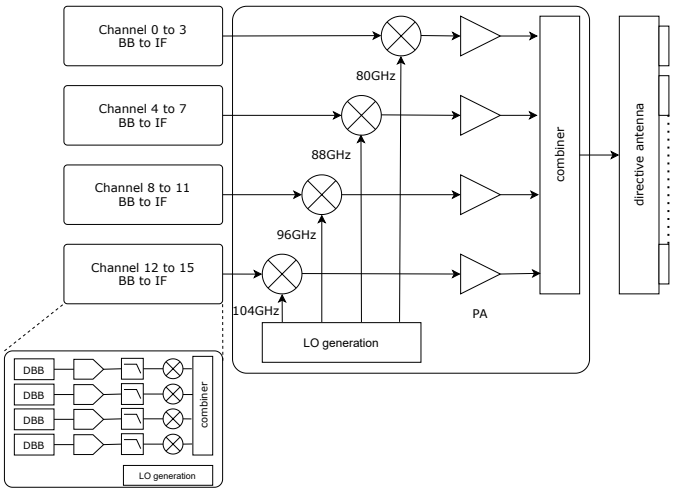

Fig. 1. D-Band Transceiver architecture

B. RF Architecture

In [5], we propose a super-heterodyne D-Band CMOS transceiver. The high level architecture is depicted in Fig. 1. The system supports 16 baseband carriers that are grouped into 4 subbands of 4 consecutive carriers. Each subband is converted to different intermediate frequency (IF) carrier in the V-Band. Then, the 4 IF bundles are up converted to the D-Band. The carriers are then combined and fed into a directive antenna. It results in a system that supports carrier aggregation in the range $125-157$ GHz. Power amplification is performed prior to combining and limit the strain on the PAs. However, combining 4 carriers together requires a large input back-off power (because of high PAPR) which limits the energy efficiency of the system. Thankfully, the DFT-s-OFDM still presents a PAPR gain (1.25 dB with probability of 10^{-5}) over the OFDM for each aggregated signal. This gain, even if it may seem small, is particularly interesting by considering the low efficiency of PAs for these bands.

The RX chain is the dual of the TX. It should be noticed that a single full-band low noise amplifier (LNA) is placed at the antenna port with limited gain to optimize the noise figure. RF and IF amplifications are performed in order to reduce the strain on the bandwidth. In addition to the original architecture and design efforts on low cost silicon technologies, a particular effort has been made on the design of a low PN local oscillator (LO) generation based on an original approach detailed in the following subsection.

C. Low PN LO Generation

The LO generation is composed of a voltage-controlled oscillator (VCO) which is periodically switched (on and off) by the input signal, providing periodically repeated oscillations train (PROT). This multi-harmonic signal is injected into an oscillator (ILO) that locks onto the harmonic of interest, providing a continuous wave sinusoidal signal. This programmable multiplication technique requires a single fixed low frequency reference to achieve multi-channel LO generation.

This technique is therefore particularly well suited to the concept of carrier aggregation presented above.

Moreover, the nature of the induced PN is also remarkable in the sense that, it is mostly generated by the injected low frequency oscillator into the ILO locking range (>1GHz) with only the multiplicative effect:

$$\text{PSD}_{LO} = \text{PSD}_{in} + 20\log_{10}\left(\frac{f_{LO}}{f_{in}}\right), \quad (1)$$

where PSD_{LO} and PSD_{in} are the power spectral density (PSD) of output (resp. input) local oscillator. f_{LO} and f_{in} are the output and input frequency of the LO. Outside the ILO locking range, the PN is the one from the ILO in free running mode ($1/f^2$ behaviour), leading to very low PN. This property is essential to address the future sub-THz and THz bands. Interested readers can refer to [5], [20], [21] for theoretical and implementation details.

III. PN Measure and Compensation Method

A. PSD Caracterization

Once the system depicted in Fig. 1 is manufactured, PN measurements can be performed with a spectrum analyzer. The generation of the LO is the same for TX and RX. The LO for the IF generates a 2.16 GHz reference signal from a phase-locked loop (PLL). The second LO outputs a 4.32 GHz clock obtained by doubling the original 2.16 GHz LO signal. The results of the measurements are shown in Fig. 2.

The PSD of the measured PN is depicted for the channels 1, 4 and 8 as well as the generic model standardized by the 3GPP [22]. In the case of 3GPP, the PN from a base station (BS) is different from that of a user equipment (UE). Indeed, for UEs, the integration and cost constraints lead to the design of lower quality and thus noisier LO. The achieved performance are quite good, especially for a CMOS system. In the $1/f^2$ region, the PSD of the measured PN is close to the 3GPP BS model (high-end). The noise floor is however a little bit higher with -115 dBc/Hz from the measurement and -119 dBc/Hz for the 3GPP one. It seems worth noticing that, the low frequency (*i.e.* near-carrier) contribution of measured noise is higher than the expected 3GPP. The theoretical PSD of the PN generated by the proposed architecture can be obtained from (1) and is depicted as well in Fig. 2.

The measured PSDs will serve as the basis for system-level evaluations of OFDM and DFT-s-OFDM performance. The generation of the PN is done by simple filtering of uncorrelated Gaussian noise by a filter representative of the PSD of the PN. The PN seen by the receiver is the combination of the PN of the transmitter and the receiver, which are not correlated each others, but which follow the same PSD.

B. PN Compensation Methods

The presence of PN is inevitable and leads to the generation of ICI as well as a common phase error (CPE) in OFDM systems [6]. In 5G-NR, phase tracking reference signal (PTRS) are added in addition to conventional demodulation reference signal (DMRS) to enhance the estimation of PN distortion [8]. When it comes to estimation algorithms, in OFDM systems we usually perform CPE Estimation (CPEE) algorithm

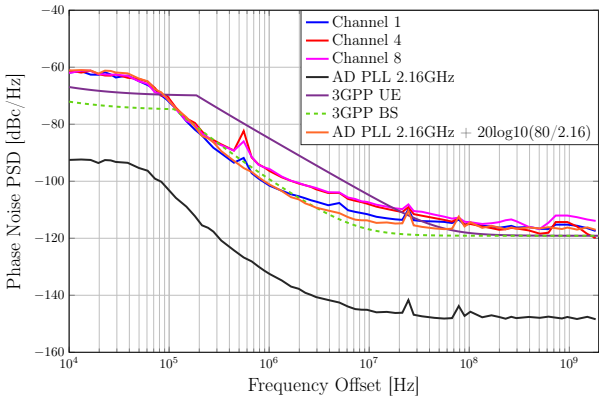

Fig. 2. Power Spectral Density PN of the 3GPP model and the measurement from the CMOS Integrated Circuit

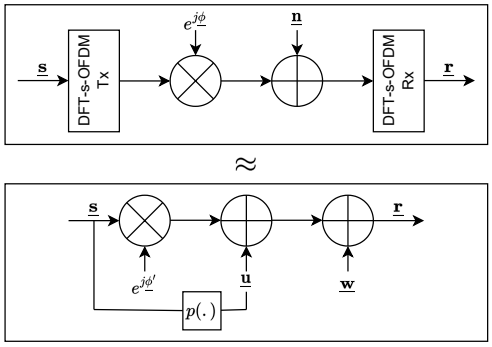

Fig. 3. DFT-s-OFDM system model with PN. The simplified model (bottom) is valid for large size of precoding. $\underline{\phi} = \underline{\phi}_{TX} + \underline{\phi}_{RX}$

which consists in a simple average over received PTRS [13]. Sometimes the CPE correction only is not sufficient, *i.e.* the ICS is not large enough to avoid negligible ICI. In that case, ICI cancellation techniques are needed [10], [12]. In the case of DFT-s-OFDM systems with large spreading, the effects of PN is different: the received signal experiences a non-constant phase rotation (*i.e.* the phase rotation is frequency dependent) and ICI appears as well but, is less noisy than OFDM. The compensation is done after de-spreading at the receiver using dedicated PTRS. The simplest method to perform the PN estimation is a linear interpolation (LI) [13]. By considering the work of [23], we propose to use a more sophisticated method based on the estimation of a Wiener interpolation filter (WIF) inspired from [14].

This technique requires the estimation of statistical properties of the PN. The PN is estimated at PTRS position. The received PTRS vector $\underline{\mathbf{r}}_\mathbf{p}$, according to the equivalent system model described in Fig. 3, can be expressed as follows:

$$\underline{\mathbf{r}}_\mathbf{p} = \mathbf{M_p}\mathbf{\Phi}\underline{\mathbf{s}} + \mathbf{M_p}\underline{\mathbf{u}} + \mathbf{M_p}\underline{\mathbf{w}}, \quad (2)$$

where $\mathbf{M_p}$ represents the PTRS sampling matrix of size $K \times N_s$. The term $\mathbf{\Phi}$ is the diagonal matrix which contains the exponential vector $e^{j\underline{\phi}'}$ on its diagonal. The vector $\underline{\phi}'$ represents the equivalent PN after DFT-s-OFDM receiver. The terms $\underline{\mathbf{s}}$, $\underline{\mathbf{u}}$ and $\underline{\mathbf{w}}$ respectively represent the transmitted symbols, the ICI and the additive thermal noise. From the

received PTRS vector, we look for a linear filter such that it satisfies the following condition:

$$\min_{\mathbf{Z}} E\left[\left\|\mathbf{Z}\underline{\mathbf{r}}_{\mathbf{p}} - e^{j\underline{\phi}'}\right\|^2\right]. \quad (3)$$

By assuming that (i) the additive noise is zero-mean, (ii) the ICI is also zero-mean, (iii) the additive noise and the ICI are independent, and (iv) the transmitted signal and the ICI are independent, then the expression of the filter $\mathbf{Z}$ solution of (3) is defined as follows

$$\mathbf{Z} = \left(\left(\mathbf{R}^H_{e^{j\underline{\phi}'}}\mathbf{M}^H_{\mathbf{p}}\right) \odot \left(\underline{\mathbf{1}}_{N_s} \cdot \underline{\mathbf{s}}^H_{\mathbf{p}}\right)\right)\mathbf{A}^{\dagger}. \quad (4)$$

The matrix $\mathbf{Z}$ is a $N_s \times K$ matrix where N_s is the size of the DFT spreading and K is the number of inserted pilots. The terms $\underline{\mathbf{s}}_{\mathbf{p}}$ represents the transmitted PTRS vector. $\mathbf{R}_{e^{j\underline{\phi}'}}$ represents the cross-correlation matrix of $e^{j\underline{\phi}'}$ and $\mathbf{A}$ defined in (5).

$$\mathbf{A} = \left(\mathbf{M}_{\mathbf{p}}\mathbf{R}^H_{e^{j\underline{\phi}'}}\mathbf{M}^H_{\mathbf{p}}\right) \odot \left(\underline{\mathbf{s}}_{\mathbf{p}}\underline{\mathbf{s}}^H_{\mathbf{p}}\right) + \mathbf{M}_{\mathbf{p}}\left(\mathbf{R}^H_{\underline{\mathbf{u}}} + \mathbf{R}^H_{\underline{\mathbf{W}}}\right)\mathbf{M}^H_{\mathbf{p}} \quad (5)$$

where $\mathbf{R}_{\underline{\mathbf{u}}}$ and $\mathbf{R}_{\underline{\mathbf{w}}}$ are respectively the cross-correlation matrices of the ICI and the thermal noise. Then, the estimated and interpolated PN is

$$\hat{\underline{\phi}}' = \arg\left(\mathbf{Z}\underline{\mathbf{r}}_{\mathbf{p}}\right), \quad (6)$$

and the expression of the received symbols after PN compensation is obtained as follows:

$$\hat{\underline{\mathbf{r}}}^{(m)} = \underline{\mathbf{r}}^{(m)}e^{-j\hat{\underline{\phi}}'^{(m)}}, \quad \forall\, m = [0, N_s - 1]. \quad (7)$$

C. Estimation of PN Stochastic Properties

The proposed method requires an *a-priori* knowledge of the cross-correlation matrices $\mathbf{R}_{e^{j\underline{\phi}'}}$ and $\mathbf{R}_{\underline{\mathbf{u}}}$. We now present here a method for estimating $\mathbf{R}_{e^{j\underline{\phi}'}}$. In the case of the DFT-s-OFDM system, the exponential vector $e^{j\underline{\phi}'}$ can be expressed as follows:

$$e^{j\underline{\phi}'} = \mathbf{diag}\left\{\mathbf{F}^H_{N_s}\mathbf{D}\mathbf{F}_N\mathbf{\Phi}_C\mathbf{F}^H_N\mathbf{M}\mathbf{F}_{N_s}\right\}, \quad (8)$$

where $\mathbf{diag}\{\cdot\}$ is the operator which returns the diagonal of a matrix. The term $\mathbf{\Phi}_C$ is the diagonal matrix containing the PN shifts $e^{j\underline{\phi}}$. The vector $\underline{\phi}$ is the sum of the PN generated by the oscillator at the transmitter and receiver. The matrices $\mathbf{M}$ and $\mathbf{D}$ respectively represent the N_s-to-N mapping matrix and the N-to-N_s demapping matrix. By posing $\mathbf{F}_{RX} = \mathbf{F}^H_{N_s}\mathbf{D}\mathbf{F}_N$ and $\mathbf{F}_{TX} = \mathbf{F}^H_N\mathbf{M}\mathbf{F}_{N_s}$, we obtain the relation below:

$$e^{j\underline{\phi}'} = \mathbf{B}e^{j\underline{\phi}} \quad \text{with} \quad \mathbf{B}^{(i,k)} = \mathbf{F}^{(i,k)}_{RX}\mathbf{F}^{(k,i)}_{TX} \quad (9)$$

with $i \in [\![1, \cdots, N_s]\!]$ and $k \in [\![1, \cdots, N]\!]$. Therefore, the cross-correlation matrix $\mathbf{R}_{e^{j\underline{\phi}'}}$ is expressed as follows

$$\mathbf{R}_{e^{j\underline{\phi}'}} = E\left[e^{j\underline{\phi}'} \cdot e^{j\underline{\phi}'^H}\right] = \mathbf{B}\mathbf{R}_{e^{j\underline{\phi}}}\mathbf{B}^H. \quad (10)$$

The matrix $\mathbf{R}_{e^{j\underline{\phi}}}$ can be obtained by using the small angle approximation $e^{j\underline{\phi}} \simeq \underline{\mathbf{1}}_N + j\underline{\phi}$:

$$\mathbf{R}_{e^{j\underline{\phi}}} \simeq E\left[\left(\underline{\mathbf{1}}_N + j\underline{\phi}\right)\left(\underline{\mathbf{1}}_N + j\underline{\phi}\right)^H\right] = \mathbf{1}_N + \mathbf{R}_{\underline{\phi}}, \quad (11)$$

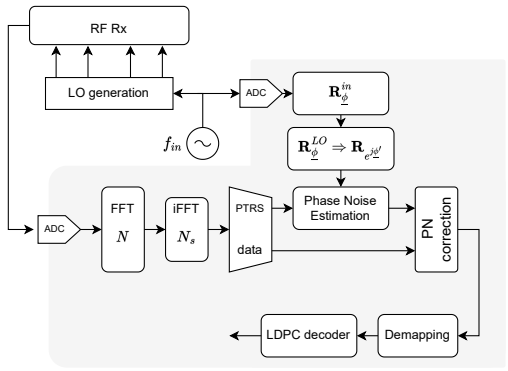

Fig. 4. Block diagram of the proposed digital baseband receiver for DFT-s-OFDM.

where $\mathbf{R}_{\underline{\phi}}$ is the cross-correlation of the PN vector generated by the oscillators. By replacing (11) in (10), we finally obtain:

$$\mathbf{R}_{e^{j\underline{\phi}'}} \simeq \mathbf{B}\left(\mathbf{1}_N + \mathbf{R}_{\underline{\phi}}\right)\mathbf{B}^H. \quad (12)$$

We thus expressed the dependence of the cross-correlation matrix to estimate $\mathbf{R}_{e^{j\underline{\phi}'}}$ with the PN property of the LO $\mathbf{R}_{\underline{\phi}}$. By assuming that the PN generated at the transmitter and receiver are zero-mean and independent, we have:

$$\mathbf{R}_{\underline{\phi}} = \mathbf{R}_{\underline{\phi}^{TX}} + \mathbf{R}_{\underline{\phi}^{RX}} \quad (13)$$

where $\mathbf{R}_{\underline{\phi}^{TX}}$ and $\mathbf{R}_{\underline{\phi}^{RX}}$ are respectively the cross-correlation matrices of the PN at the transmitter and receiver. They can be estimated at both the transmitter and receiver.

The block diagram of the proposed receiver is depicted in Fig. 4. The received IQ samples, once synchronized in time and frequency, are processed by a DFT-s-OFDM receiver. Then, PTRS are extracted and feed the PN estimation block. The cross-correlation matrix $\mathbf{R}^{in}_{\underline{\phi}}$ is derived from the sampling of the low frequency oscillator and then the estimation filter is derived. Considering our architecture, by applying (1), one obtains:

$$\mathbf{R}_{\underline{\phi}^{RX}} = \mathbf{R}^{LO}_{\underline{\phi}} = \left(\frac{f_{LO}}{f_{in}}\right)^2 \mathbf{R}^{in}_{\underline{\phi}}, \quad (14)$$

where $\mathbf{R}^{in}_{\underline{\phi}}$ represents the cross-correlation matrix of the PN generated at the low frequency f_{in}. The proposed solution is limited to the receiver but, it is also necessary to know the statistics of the PN at the transmitter. This can be done either by an information exchange, or by other methods such as blind estimation. However, they are out of the scope of this work. Similarly, the TX LO at BS should have a better quality than the UE RX. In this way, the PN at the BS can be known *a-priori*, especially if the TX must respect a certain quality given by a standard. In the following, we assume that the PN at the transmitter and receiver follows the same law, *i.e.* $\mathbf{R}_{\underline{\phi}} = 2\mathbf{R}_{\underline{\phi}^{RX}}$.

Remark 1*:* It should also be mentioned that the calculation of the interpolation filter requires the knowledge of the cross-correlation of the PN-induced ICI. This quantity is difficult to estimate in practice. If the receiver is in a regime where the noise contribution exceeds the ICI power, the ICI term can be neglected. As a consequence, regarding the targeted spectral efficiencies, we assume that $\mathbf{R}_{\underline{\mathbf{u}}} = \mathbf{0}_{N_s}$.

TABLE II
SIMULATION PARAMETERS

Sampling Frequency	F_s	3932.16 MHz
Numerology	μ	5 to 10 - Option 2
Signal bandwidth	B	1884.32 MHz
Carrier frequency	F_c	140 GHz
PN model		measured
Tx IFFT size	N	$4096 \times 2^{-\mu+6}$
Number of active carriers	N_s	$12\left\lfloor \frac{B}{12F_s}N \right\rfloor$
LDPC coding rate	CR	$0.3, 0.5, 0.7$ and 0.9
LDPC decoder		Layered Min-Sum, 15 iterations
Modulation	M	4, 16 and 64 QAM

Remark 2***:*** All the analytical expressions presented in this section are based upon the assumption of an additive white Gaussian noise (AWGN) channel, thanks to the use of high gain and highly directive antennas which spatially filter multi paths.

IV. NUMERICAL EVALUATIONS

a) ***Assumptions****:* In this section, we describe the performance evaluation of a 5G-NR PHY layer waveform with measured PN. Simulation parameters are described into TABLE II. For all the configurations, we assume a sampling frequency of 3.93216GHz and a signal bandwidth of 1.8 GHz. The 5G-NR numerologies are used and extended numerologies following "Option 2" in TABLE I are considered. In this case, the ICS is increased while maintaining a constant sampling rate (*i.e.* the size of FFT is reduced). The generated PN is following the PSD of the "Channel 1" in Fig. 2. The signal-to-noise ratio (SNR) is evaluated on the full signal bandwidth, *i.e.* 3.93216 GHz. Regarding the PTRS, they are continuous reference symbols and are spaced every 8 subcarriers. For all our simulations, received pilots are noisy. Low-density parity-check (LDPC) codes are considered for the channel coding.

b) ***OFDM with CPEE****:* Fig. 5 presents the performance of an OFDM system for different modulation orders and numerologies. We evaluate the SNR ratio value that achieves the target transport block error rate (TBLER) of 10^{-2}. We consider three levels: (i) low spectral efficiency (SE) with QPSK and coding rate (CR) of $\{0.3, 0.5, 0.7\}$ and (16-QAM,0.3); (ii) medium SE with (QPSK,0.9) and 16-QAM with CR=$\{0.5, 0.7\}$; and (iii) high SE which includes 64-QAM with CR=$\{0.5, 0.7, 0.9\}$. One can observe that for the low and medium SE, all the numerologies provide approximately the same SNR value, except in the case of (16-QAM,0.7) where we observe a SNR gap of 0.5 dB for the numerology 5 compared to the others. For the high SE, one can observe that for the numerology 5 and 6, the SNR values increase until the target TBLER cannot be achieved. Indeed, when we increase the SE, the ICS is no longer sufficient and the ICI then starts to be disturbing. Therefore, if we plan to use 5G-NR numerologies in high SE, in addition to the CPE correction, ICI cancellation techniques are needed. Alternatively, the numerology can be increased (*i.e.* increase the ICS) following "Option 2".

c) ***DFT-s-OFDM with proposed algorithm****:* When it comes to DFT-s-OFDM, two algorithms are evaluated: first, a simple LI is performed on the phase estimation realized on each pilot position. Second, the proposed WIF algorithm

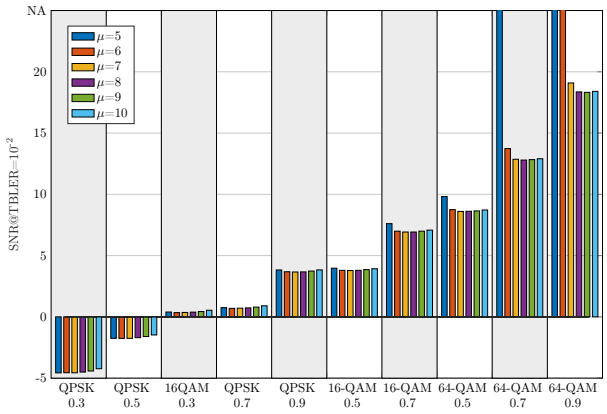

Fig. 5. SNR [dB] values to achieve a TBLER of 10^{-2} for an OFDM system assuming different numerologies and a pilot density of 6%. "NA" stands for "Non achievable".

is applied. In a first embodiment, we consider a perfect statistical knowledge of the PN statistic $\mathbf{R}_{e^{j\underline{\Phi}'}}$: "WIF genie-aided". Fig. 6 depicts the TBLER versus SNR for DFT-s-OFDM and OFDM waveforms. For DFT-s-OFDM and numerologies $\mu = \{5, 6, 7\}$, the proposed WIF algorithm outperforms the LI algorithm. The LI is noise sensitive and does not allow efficient phase denoising. Furthermore, we observe that the DFT-s-OFDM with WIF algorithm outperforms the OFDM with CPE correction for the numerology $\mu = 5$. For $\mu = 6$, one can observe that the DFT-s-OFDM with WIF algorithm outperforms once again OFDM with CPE correction considering the 64-QAM modulation order and a CR=$\{0.7, 0.9\}$. Finally for $\mu = 7$, both DFT-s-OFDM with WIF algorithm and OFDM with CPE correction provides the same performance. Therefore, the DFT-s-OFDM with the WIF algorithm could be a solution in case we consider the current 5G-NR waveform and today numerologies.

We also perform the WIF algorithm by estimating the PN statistics. We first estimate the cross-correlation matrix $\mathbf{R}_{\underline{\Phi}}^{in}$ of the low frequency oscillator and then, we derive the cross-correlation matrix $\mathbf{R}_{\underline{\Phi}^{RX}}$ by using the expression in (14) and then we compute $\mathbf{R}_{\underline{\Phi}}$. Finally, we obtain the right cross-correlation for the WIF algorithm $\mathbf{R}_{e^{j\underline{\Phi}'}}$ with the expression (12). As highlighted in Fig. 6, the WIF algorithm with the estimated cross-correlation matrix $\mathbf{R}_{e^{j\underline{\Phi}'}}$ gives the same performance as the one with its perfect knowledge. This result validates the possibility to implement the WIF algorithm by estimating the cross-correlation matrix.

V. CONCLUSION

The proposed work takes an interesting approach mixing RF circuit and signal processing designs. We observed that the numerology system, specified up to 960 kHz in 5G-NR standard, reaches its limits in sub-THz bands. We showed that for the OFDM waveform, either larger ICS is required for using only a low compexity algorithm such as CPE correction, or ICI cancellation techniques by keeping standard 5G-NR numerologies. We demonstrated that the use of the WIF algorithm based on the statistic properties of the correlated nature of the PN, leads to a significant performance gain in DFT-s-OFDM systems with a real measured PN PSD, considering

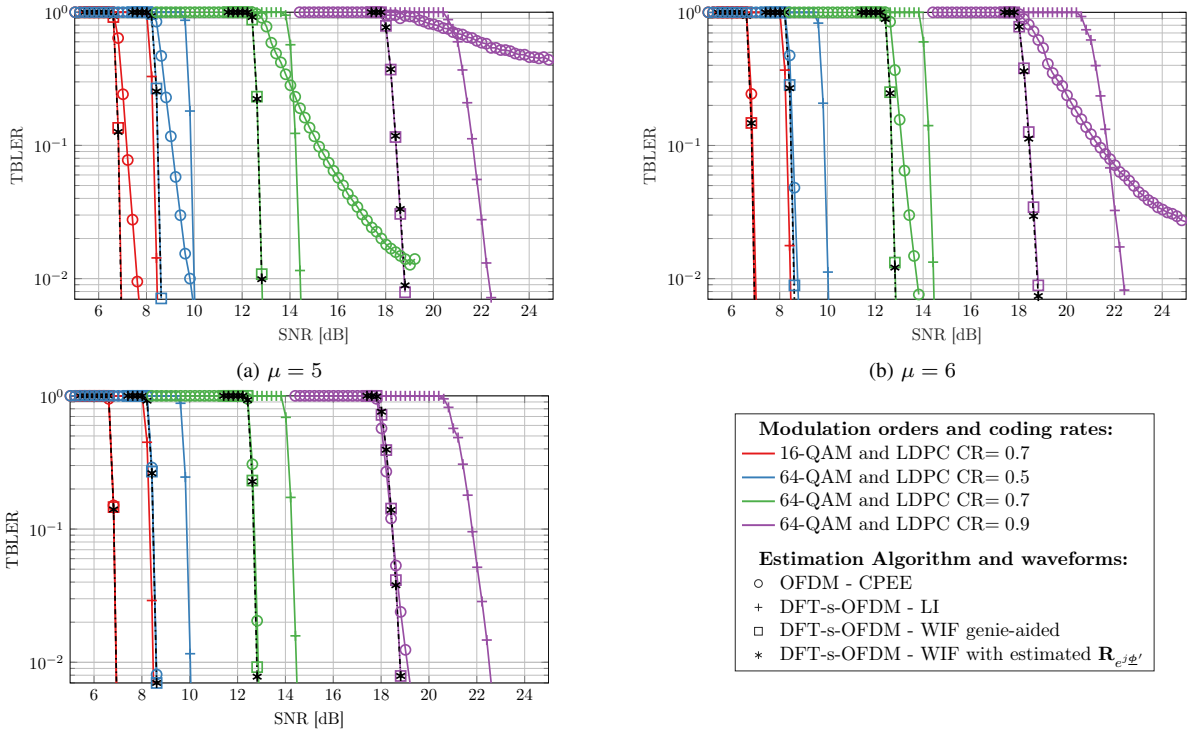

(a) $\mu = 5$

(b) $\mu = 6$

(c) $\mu = 7$

Fig. 6. Performance of a DFT-s-OFDM and OFDM systems in terms of TBLER in function of SNR considering the numerologies $\mu = \{5, 6, 7\}$.

standard 5G-NR numerology. We showed how to estimate the desired PN statistics directly by sampling the reference low frequency LO according to the presented architecture. As a consequence, thanks to its reduced PAPR and improved PN robustness with the proposed WIF compensation, DFT-s-OFDM stands as a strong contender to be considered for sub-THz communications. As a perspective to this work, we will implement the WIF algorithm in a realistic RF transmission scenario.

REFERENCES

[1] A. I. Salameh and M. El Tarhuni, "From 5G to 6G-Challenges, Technologies, and Applications," *MDPI Future Internet*, vol. 14, no. 4, 2022.

[2] J.-B. Doré, Y. Corre, S. Bicais *et al.*, "Above-90GHz Spectrum and Single-Carrier Waveform as Enablers for Efficient Tbit/s Wireless Communications," in *Proc. Int. Conf. on Telecommun. (ICT'2018)*, Saint-Malo, France, Jun. 2018.

[3] S. Voinigescu, M. Khanpour, S. Nicolson *et al.*, "CMOS receivers in the 100–140 GHz range," in *Proc. IEEE MTT-S Int. Microwave Symp. Digest*, 2009, pp. 193–196.

[4] N. Deferm, W. Volkaerts, J. F. Osorio *et al.*, "A 120GHz fully integrated 10Gb/s wireless transmitter with on-chip antenna in 45nm low power CMOS," in *Proc. European Conference on Solid-State Circuits (ESSCIRC)*, 2013, pp. 331–334.

[5] J. González-Jiménez, A. Siligaris, A. Hamani *et al.*, "Channel Bonding Transceivers for Efficient 100 Gb/s and Beyond Wireless and Plastic Waveguide Communications," in *Proc. IEEE Int. Conf. on Electron., Circuits and Syst. (ICECS)*, 2022, pp. 1–4.

[6] A. Garcia Armada, "Understanding the effects of phase noise in orthogonal frequency division multiplexing (OFDM)," *IEEE Trans. on Broadcast.*, vol. 47, no. 2, pp. 153–159, 2001.

[7] O. Tervo, I. Nousiainen, I. P. Nasarre *et al.*, "On the Potential of Using Sub-THz Frequencies for Beyond 5G," in *Proc. Joint Eur. Conf. on Netw. and Commun. & 6G Summit (EuCNC/6G Summit)*, 2022, pp. 37–42.

[8] T. Levanen, O. Tervo, K. Pajukoski *et al.*, "Mobile Communications Beyond 52.6 GHz: Waveforms, Numerology, and Phase Noise Challenge," *IEEE Wireless Commun.*, vol. 28, 2021.

[9] D. Petrovic, W. Rave, and G. Fettweis, "Intercarrier interference due to phase noise in OFDM - estimation and suppression," in *Proc. IEEE Veh. Technol. Conf. (VTC-Fall)*, 2004, pp. 2191–2195.

[10] M. Afshang, D. Hui, J.-F. T. Cheng *et al.*, "On Phase Noise Compensation for OFDM Operation in 5G and Beyond," in *Proc. IEEE Wireless Commun. and Netw. Conf. (WCNC)*, 2022, pp. 2166–2171.

[11] J.-C. Sibel, "Tracking the phase noise in sub-THz bands," in *Proc. IEEE Wireless Commun. and Netw. Conf. (WCNC)*, 2022, pp. 932–937.

[12] J. L. Hernando, A. S. Tan, and A. Shojaeifard, "Mitigation of Phase Noise-induced ICI at THz bands using CP-OFDM PT-RS signals," in *Proc. IEEE Globecom Workshops*, 2022, pp. 1766–1771.

[13] J.-C. Sibel, "Pilot-Based Phase Noise Tracking for Uplink DFT-s-OFDM in 5G," in *Proc. Int. Conf. Telecommunications (ICT)*, 2018, pp. 52–56.

[14] Y. Bello, J.-B. Doré, and D. Demmer, "DFT-s-OFDM for sub-THz Transmission - Tracking and Compensation of Phase Noise," in *Proc. IEEE Consum. Commun.& Netw. Conf. (CCNC)*, 2023.

[15] 3GPP, "NR: Physical channels and modulation," Tech. Spec. Group Radio Access Netw. Rel. 17 TS 38.211 v. 17.1.0, 2022-April.

[16] L. Pometcu and R. D'Errico, "An Indoor Channel Model for High Data-Rate Communications in D-Band," *IEEE Access*, pp. 9420–9433, 2020.

[17] N. Dinur and D. Wulich, "Peak to average power ratio in amplitude clipped high order OFDM," in *Proc. IEEE Mil. Commun. Conf. (MILCOM)*, vol. 2, 1998, pp. 684–687 vol.2.

[18] G. Berardinelli, K. I. Pedersen, T. B. Sorensen *et al.*, "Generalized DFT-Spread-OFDM as 5G Waveform," *IEEE Commun. Mag.*, pp. 99–105, 2016.

[19] B. Murmann, "ADC Performance Survey 1997-2022," [Online]. Available: https://github.com/bmurmann/ADC-survey.

[20] C. Jany, A. Siligaris, J. L. Gonzalez-Jimenez *et al.*, "A Programmable Frequency Multiplier-by-29 Architecture for Millimeter Wave Applications," *IEEE J. of Solid-State Circuits*, vol. 50, 2015.

[21] A. Hamani, F. F. Manzillo, A. Siligaris *et al.*, "A 56.32 Gb/s 16-QAM D-band Wireless Link using RX-TX Systems- in-Package with Integrated Multi-LO Generators in 45nm RFSOI," in *Proc. 2022 IEEE Radio Freq. Integrated Circuits Symp. (RFIC)*, 2022, pp. 75–78.

[22] 3GPP, "Study on new radio access technology: Radio Frequency (RF) and co-existence aspects," TS 38.803, 2017-09.

[23] M. Chung, L. Liu, and O. Edfors, "Phase-Noise Compensation for OFDM Systems Exploiting Coherence Bandwidth: Modeling, Algorithms, and Analysis," *IEEE Trans. on Wireless Commun.*, vol. 21, no. 5, pp. 3040–3056, 2022.